

Epidermolysis Bullosa Simplex-Type Mutations Alter the Dynamics of the Keratin Cytoskeleton and Reveal a Contribution of Actin to the Transport of Keratin Subunits

Nicola Susann Werner,* Reinhard Windoffer,[†] Pavel Strnad,[†]
Christine Grund,[‡] Rudolf Eberhard Leube,[†] and Thomas Michael Magin*[§]

*Institut fuer Physiologische Chemie, Abteilung fuer Zellbiochemie, Universitaetsklinikum Bonn, 53115 Bonn, Germany; [†]Division of Cell Biology, German Cancer Research Center, 69120 Heidelberg, Germany; and [‡]Department of Anatomy, Johannes Gutenberg-University, D-55128 Mainz, Germany

Submitted September 24, 2003; Revised October 20, 2003; Accepted October 31, 2003
Monitoring Editor: Richard Hynes

Dominant keratin mutations cause epidermolysis bullosa simplex by transforming keratin (K) filaments into aggregates. As a first step toward understanding the properties of mutant keratins in vivo, we stably transfected epithelial cells with an enhanced yellow fluorescent protein-tagged K14R₁₂₅C mutant. K14R₁₂₅C became localized as aggregates in the cell periphery and incorporated into perinuclear keratin filaments. Unexpectedly, keratin aggregates were in dynamic equilibrium with soluble subunits at a half-life time of <15 min, whereas filaments were extremely static. Therefore, this dominant-negative mutation acts by altering cytoskeletal dynamics and solubility. Unlike previously postulated, the dominance of mutations is limited and strictly depends on the ratio of mutant to wild-type protein. In support, K14R₁₂₅C-specific RNA interference experiments resulted in a rapid disintegration of aggregates and restored normal filaments. Most importantly, live cell inhibitor studies revealed that the granules are transported from the cell periphery inwards in an actin-, but not microtubule-based manner. The peripheral granule zone may define a region in which keratin precursors are incorporated into existing filaments. Collectively, our data have uncovered the transient nature of keratin aggregates in cells and offer a rationale for the treatment of epidermolysis bullosa simplex by using short interfering RNAs.


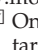
INTRODUCTION

Intermediate filaments (IFs), in concert with microtubules (MTs) and microfilaments (MFs), play important roles in the organization and mechanical integrity of cells (Fuchs and Cleveland, 1998). Mutations in genes coding for K5 and K14 cause the human skin disorder epidermolysis bullosa simplex (EBS) (Irvine and McLean, 1999). In the majority of patients, the severe Dowling Meara disease variant results from a conserved mutation in the coil 1A region of the K14 rod domain at codon 125, leading to an exchange of R to C or H. This causes a collapse of keratin filaments and the fragility of basal keratinocytes. The phenotypic consequences of K5 and K14 mutations comprise blistering of the skin upon mild trauma and substantial abnormalities in keratin assembly in humans and in mouse models (for review, see Coulombe and Omary, 2002) becoming evident by

the formation of electron-dense keratin aggregates in tissues (Anton-Lamprecht and Schnyder, 1982) and in patient-derived primary keratinocytes (Kitajima *et al.*, 1989; Coulombe *et al.*, 1991a). However, the underlying molecular mechanisms are still poorly understood. The formation of apparently stable protein inclusions has been considered as gain of toxic function, being more severe than the loss of the filaments. This has been accorded to the dominant-negative effect of EBS hot-spot mutations, which are considered to exacerbate the fragility of the cytoskeleton because of the existence of fatal, insoluble debris in the cells (Fuchs and Cleveland, 1998). In fact, aggregates caused by EBS hot-spot mutations differ from particles observed during the process of mitosis (Windoffer and Leube, 2001), with respect to their localization in the cell-cell periphery versus whole cytoplasm; and their origin, mutation-specific rupture of the cytoskeleton versus regulated phosphorylation events during the cell cycle. Therefore, the treatment of EBS presents a major challenge and may have to revert the formation of aggregates.

The assembly of apolar IF in cells, in contrast to the directional assembly of MF and MT (Rosenbaum, 2000; Amann and Pollard, 2001; Small *et al.*, 2002), is not understood. Although in vitro assembly of IF proceeds without accessory proteins (Quinlan *et al.*, 1985; Herrmann *et al.*, 2002), recent evidence supports the notion that in vivo, motor proteins, plakin family proteins, energy, and post-translational modifications may play a significant role in the

Article published online ahead of print. Mol. Biol. Cell 10.1091/mbc.E03-09-0687. Article and publication date are available at www.molbiolcell.org/cgi/doi/10.1091/mbc.E03-09-0687.

  Online version of this article contains video and supplementary material for some figures. Online version is available at www.molbiolcell.org.

[§] Corresponding author. E-mail address: t.magin@uni-bonn.de.
Abbreviations used: EBS, epidermolysis bullosa simplex; EYFP, enhanced yellow fluorescent protein; IF, intermediate filament; K, keratin; MF, microfilament; MT, microtubule; mut, mutant; wt, wild type.

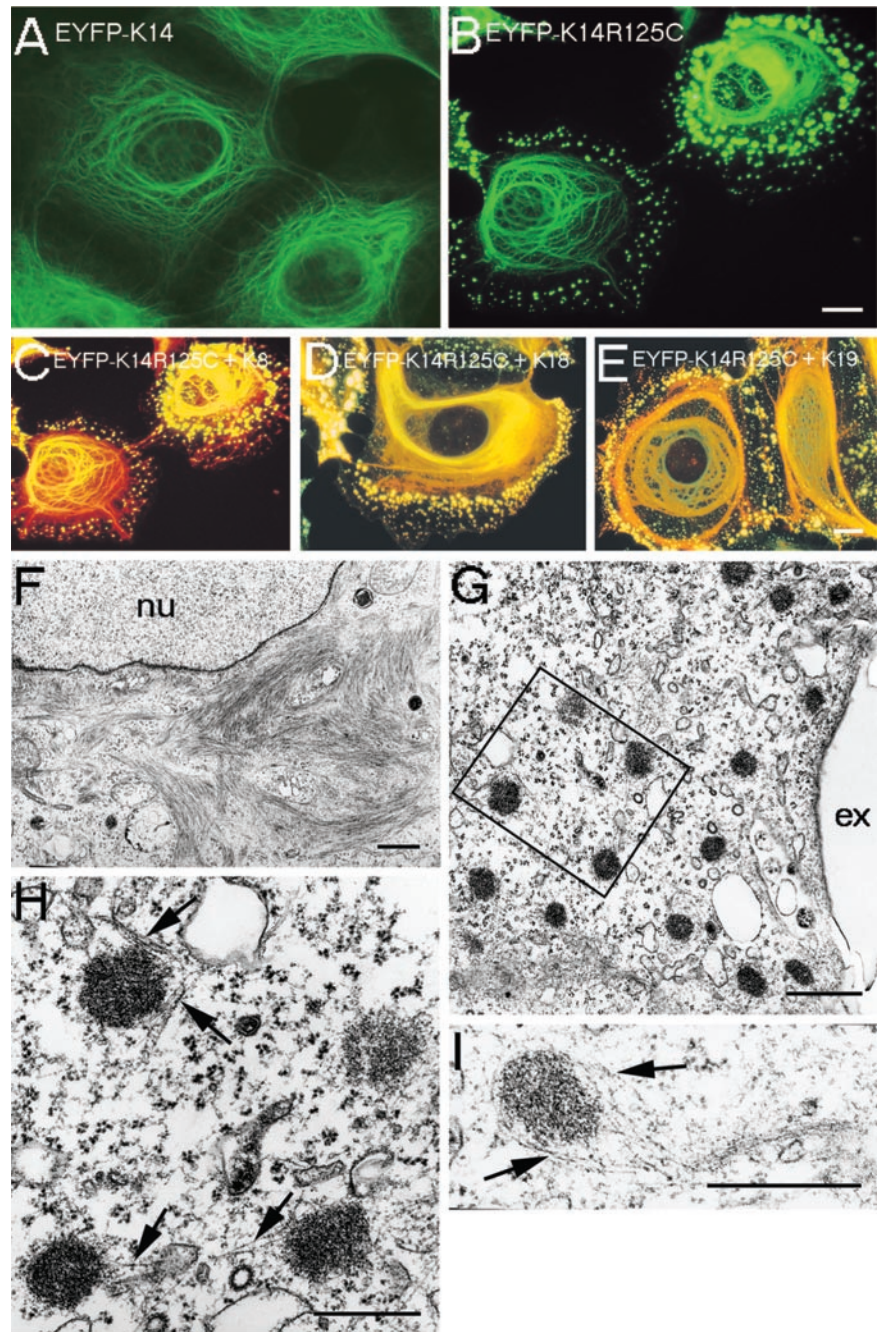


Figure 1. Double fluorescence and transmission electron microscopy of wt and mut MCF-7 cells. Stable expression of EYFP-K14 (A), EYFP-K14R₁₂₅C (B); merged images of EYFP-K14R₁₂₅C and indirect immunofluorescence of K8 (C), K18 (D), and K19 (E). Electron microscopy of EYFP-K14R₁₂₅C cells shows perinuclear filaments (F) and aggregates in the cell periphery (G). (H) Higher magnification of the marked area in F. (I) Single aggregate. The arrows mark keratin filaments in close association with aggregates; nu, nucleus; ex, extracellular. Bars, 10 μ m (same magnification in A and B and C–E), 2 μ m (F), 1 μ m (G), and 0.5 μ m (H and I).

formation, maintenance, and organization of IF cytoskeletons (Chou *et al.*, 2001; Leung *et al.*, 2002). The initiation of filament assembly has been suggested to occur close to the plasma membrane (Martys *et al.*, 1999; Windoffer and Leube, 1999, 2001). Although keratins are highly insoluble (Soellner *et al.*, 1985; Chou *et al.*, 1993; Bachant and Klymkowsky, 1996) and have been assumed to form very stable structures, recent studies, by using green fluorescent protein (GFP)-tagged IFs revealed that IFs are remarkably dynamic with respect to their assembly properties and organization (Chou *et al.*, 2001). Active transport processes were reported: GFP-vimentin particles in transiently transfected migrating or spreading cells moved outward from the cell center or displayed bidirectional tracks relying on MT-based motor pro-

teins (Gyoeva and Gelfand, 1991; Ho *et al.*, 1998; Prahlad *et al.*, 1998; Yoon *et al.*, 1998; Kreitzer *et al.*, 1999; Helfand *et al.*, 2002). The limited number of studies on the motile properties of keratin particles have revealed that keratins behave different from vimentin and emphasized that GFP-keratin granules moved from the cell periphery inwards (Windoffer and Leube, 1999, 2001; Yoon *et al.*, 2001). The motility of those wild-type (wt) keratin precursors was dependent on MTs. Whether transport of IF subunits involves a direct interaction with motor or adaptor proteins is not yet known.

Because all studies on IF motility have focused on wt IF, we have set out to analyze the assembly and dynamic properties of an EYFP-tagged K14R₁₂₅C mutant in living cells because of the obvious keratin organization defects in EBS

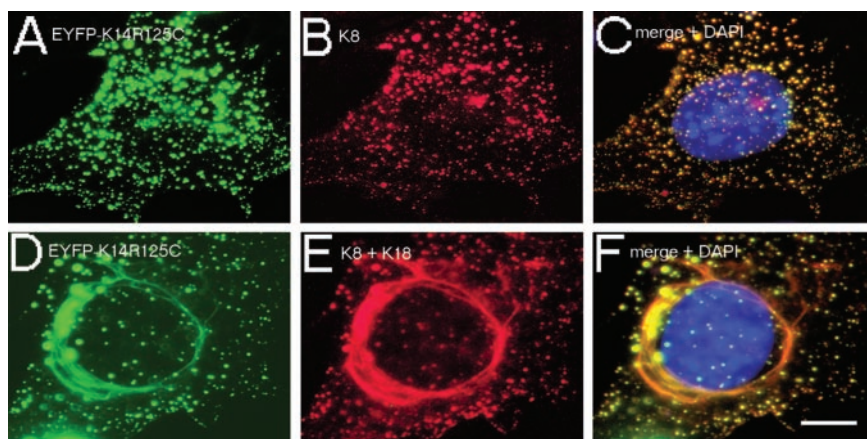


Figure 2. De novo assembly properties of mutant K14 in 3T3-L1 preadipocytes. Double fluorescence analysis of transiently transfected EYFP-K14R₁₂₅C (A and D), together with K8 (B), or K8 and K18 (E). Merged images with additional 4,6-diamidino-2-phenylindole staining of DNA are presented in C and F. Bar, 10 μ m.

patients. Stably transfected human HaCaT keratinocytes, MCF-7 breast carcinoma, and colon carcinoma HCT116 cells all displayed indistinguishable phenotypes despite their different endogenous keratin composition. Using live cell fluorescence imaging, we investigated for the first time the formation of disease-type keratin aggregates in cultured cells under steady-state conditions. MF- and MT-depolymerizing drugs were applied to study transport processes of keratin filament precursors in living cells. Via transfection of a K14R₁₂₅C-specific siRNA, we addressed possible new avenues for the therapy of EBS.

MATERIALS AND METHODS

DNA Cloning

To generate expression constructs for wt and mutant (mut) K14 fusion proteins tagged with enhanced yellow fluorescent protein (EYFP), a human K14 cDNA (kindly provided by H. Herrmann, German Cancer Research Center, Heidelberg, Germany) was amplified with primers 5'-GAATTCGATGAC-TACCTGCAGCCG-3' and 5'-GGATCCTCAGTCTTGGTCCGAAGG-3', adding flanking EcoRI and BamHI sites, respectively, and cloned into the EcoRI/BamHI restricted pEYFP-C1 vector (BD Biosciences Clontech, Palo Alto, CA). The K14R₁₂₅C mutation was created using the QuikChange site-directed mutagenesis kit (Stratagene, Amsterdam, The Netherlands) and the forward and reverse primer (5'-GAACCTCAATGACTGCCTGGCTCCTAC-3') and 5'-GTAGGAGGCCAGGCAGTCATTGAGGTTTC-3', respectively, and was verified by sequence analysis. The immediate early promoter of cytomegalovirus drove expression of wt or mutant K14 fused to EYFP at its amino terminus, and a neomycin-resistance cassette was present for selection. Constructs used for K8 and K18 expression were hCK8-LK440 and hCK18-LK440 (Bader *et al.*, 1991).

Cell Culture and Transfection Procedures

Human HaCaT keratinocytes (kindly provided by P. Boukamp, German Cancer Research Center, Heidelberg), human HCT116 cell (ATCC no. CCL-247), human MCF-7 cells, and human 3T3-L1 preadipocytes (both kindly provided by W. Franke, German Cancer Research Center, Heidelberg, Germany) were passaged in DMEM supplemented with 10% fetal calf serum (both from Invitrogen, Karlsruhe, Germany). Purified plasmid DNA was transfected into cells by using a modified calcium phosphate precipitation method (Leube *et al.*, 1989). Transiently transfected cells were analyzed 24, 48, and 72 h after transfection, and stably transfected cells were selected upon addition of 600 μ g/ml geneticin (Invitrogen). Individual colonies were isolated by cloning rings and subcloned for subsequent analyses. During inhibitor studies, cells were cultivated either with 20–40 μ M nocodazole, 10 μ M latrunculin B, or 200 μ M cytochalasin D.

Immunofluorescence and Electron Microscopy

Electron (Reichelt *et al.*, 2001) and indirect immunofluorescence microscopy (Windoffer and Leube, 1999) were performed as described previously. For F-actin staining, cells were fixed with 3.7% paraformaldehyde/phosphate-buffered saline (Sigma-Aldrich, St. Louis, MO) for 10 min at room temperature, extracted with 0.1% saponine (Calbiochem, San Diego, CA), and incubated with Alexa 594A-conjugated phalloidin (Molecular Probes Europe BV, Leiden, The Netherlands). Coverslips were examined with a fluorescence

photomicroscope (Axiophot 2E; Carl Zeiss, Jena, Germany) at room temperature, equipped with Zeiss Plan-Neofluar 63 \times /1.25 and 40 \times /1.30 oil immersion objectives and recorded with a digital camera (AxioCam color; Carl Zeiss). Image analysis and image processing were performed using the Axiovision 2.05 (Carl Zeiss) and Adobe Photoshop 6.0 software (Adobe Systems, Mountain View, CA).

Western Blotting

Total protein extracts (T) were prepared as described previously (Reichelt *et al.*, 1999) and subjected to SDS-PAGE. IF-enriched cytoskeletal extracts were prepared by cytolysis of confluent cell cultures with ice-cold low-salt buffer (10 mM Tris-HCl, pH 7.6, 140 mM NaCl, 5 mM EDTA, 5 mM EGTA, 0.5% Triton X-100, 2 mM phenylmethylsulfonyl fluoride), a subsequent centrifugation step to separate the soluble cytoskeletal fraction (S) from the insoluble cytoskeletal fraction (C), which was then resuspended in ice-cold high-salt buffer (10 mM Tris-HCl, pH 7.6, 140 mM NaCl, 1.5 M KCl, 5 mM EDTA, 5 mM EGTA, 1% Triton X-100, 2 mM phenylmethylsulfonyl fluoride), homogenized, pelleted by centrifugation, and treated like total protein extracts.

Antibodies

The following primary antibodies were used: JL-8 against EYFP (BD Biosciences Clontech), AF 138 against K5 (Babco, Richmond, CA), α -K14 and CK14.2 [kindly provided by M. Blessing (University of Mainz) and L. Langbein (German Cancer Research Center)], Ks 8.07 and Ks 18.04 against K8 and K18, respectively (Progen, Heidelberg, Germany), CK.5 against K18 (Sigma-Aldrich), TROMA-3 and LP2K against K19 (kindly provided by R. Kemler [MPI, Freiburg, Germany] and F.C. Ramaekers [University Hospital Nijmegen, Nijmegen, The Netherlands]), DP2.15 against desmoplakin (Progen), mAb-121 against plectin (kindly provided by K. Owaribe, Nagoya University, Japan), α -vinculin (Sigma-Aldrich), and α -tubulin (Sigma-Aldrich). Secondary antibodies were Cy3-conjugated and horseradish peroxidase-coupled goat α -rabbit, α -mouse, α -guinea pig, and α -rat sera (Dianova, Hamburg, Germany).

Time-Lapse Fluorescence Microscopy and Visualizations

Live cell microscopy was performed as described previously (Windoffer and Leube, 2001). To compute time-space diagrams, selected areas of interest were chosen from the recordings and imported into Amira (TGS, Düsseldorf, Germany). The data were compiled, producing superpositions that present the surface of individual fluorescent granules in time and space.

To generate time-dependent color-coded tracks of fluorescent granules, a custom-made ImagePro Plus (Media Cybernetics, Göttingen, Germany) macro was applied to image stacks of selected areas of interest.

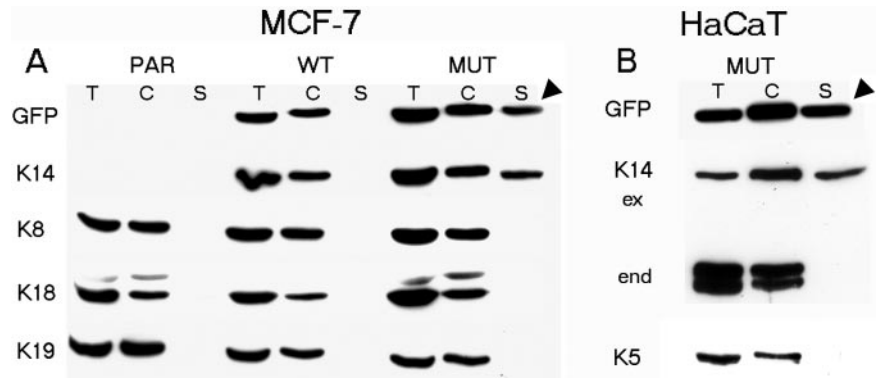
Osmotic Shock

This stress assay was performed as described previously (D'Alessandro *et al.*, 2002).

RNA Interference (RNAi)

RNAi was performed as described previously (Elbashir *et al.*, 2001; Harborth *et al.*, 2001). EYFP, K14, K14R₁₂₅C, and firefly luciferase control small interfering RNAs (siRNAs) were generous gifts of K. Weber (MPI, Göttingen, Germany). The accession numbers given below in parentheses are from GenBank. EYFP-1 (1): 5'-AAGACCCGCGCCGAGGUGAAG-3'; the siRNA sequence was from position 934–954 relative to the start codon (U55763); EYFP-2 (2): 5'-AAGAACGGCAUCAAGGUGAAC-3' (U55763) 1087–1107; K14-1 (4): 5'-AAGGAUGCCGAGGAAUGGUUC-3' (BC002690) 898–918;

Figure 3. Western blot analysis of wt and mut epithelial cells. Total protein extracts (T), insoluble cytoskeletal (C), and soluble fractions (S) were prepared from wt or mut EYFP-K14 cells and their corresponding parental cell lines. (A) Immunoblot analysis of MCF-7 (PAR) and transfected wt (WT) and mut (MUT) cells with antibodies to GFP, K14, K8, K18, and K19. (B) Immunoblot analysis of mutant-transfected HaCaT cells with antibodies to GFP, K14, and K5. The grouping of images was arranged from different gels. The arrowheads mark the soluble cytoskeletal fractions containing exclusively mut keratin. ex, exogenous K14; end, endogenous K14.



K14-2 (5): 5'-AAGCAUCCUGGAGAAGAGCC-3 (BC002690) 1055-1075); and K14R₁₂₅C (3): 5'-AACCUCAAUGACUGCCUGGCC-3' (BC002690) 361-381.

RESULTS

Spatially Restricted Aggregate Formation Reveals the Limited Effect of Dominant Keratin Mutations in Epithelial Cells

We stably transfected human epithelial MCF-7 cells, HaCaT keratinocytes, and colon carcinoma HCT116 cells with the Dowling-Meara hot-spot mutations K14R₁₂₅C (this report) and K14R₁₂₅H (our unpublished data). To study the effects of these mutations on cytoskeletal integrity in live cells, wt K14 and mut K14R₁₂₅C/H cDNAs were cloned into a mammalian expression vector tagged with EYFP at the amino terminus of K14. EYFP-imaging revealed that all cell lines expressing K14R₁₂₅C displayed a keratin pattern similar to primary EBS-keratinocytes independently of their endogenous keratin expression (Kitajima *et al.*, 1989; Coulombe *et al.*, 1991a,b; Letai *et al.*, 1993): keratin aggregates segregated to a distinct site toward the cell periphery, whereas densely packed keratin bundles were oriented in a perinuclear manner (Figure 1, B–G), a phenotype never observed in cells transfected with wt K14 (Figure 1A). The amounts of exogenously expressed wt and mut EYFP-K14 fusion proteins were similar. Thus, keratin aggregates in mut cells do not represent artifacts of overexpression or result from the EYFP-tag. Moreover, mut cells proceeded normally through all mitotic stages revealing typical M-phase-specific aggregates indistinguishable from those of wt cells (Windoffer and Leube, 2001). In the course of cytokinesis, they reformed to EBS-aggregates (our unpublished data). Immunofluorescence analysis with antibodies to the endogenous keratins K5, K14 (HaCaT), K8, K18, and K19 (MCF-7 and HCT116) revealed an overlapping pattern of transfected and endogenous keratins: aggregates and filaments not only contained the mut protein but also all endogenous keratins. We noted that some aggregates contained short EYFP-labeled filaments in their perimeter. These were further analyzed by transmission electron microscopy (Figure 1, H and I, arrows). These results confirmed the normal appearance of the mut perinuclear filaments at the ultrastructural level (Figure 1F), indicating that filament formation was not completely impaired in mut cells, and revealed the dense, granular appearance of the keratin aggregates near the cell periphery. Distinct keratin filaments were in close association with aggregates connecting them or even forming longer keratin tails. Thus, the mut protein induced aggregates accompanied by short filaments preferentially in the cell periphery in all three cell lines examined.

De Novo Keratin Assembly in Keratin-Free Cells Reveals an Assembly Defect of the EBS Hot-Spot Mutation In Vivo

Because ultrastructural analysis pointed to incomplete filament formation in mut cells, we studied the de novo assembly of the mut type I with a wt type II partner in 3T3-L1 preadipocytes that express vimentin as sole IF protein. In agreement with former studies (Bader *et al.*, 1991), wt keratins formed a normal cytoskeleton in transiently transfected 3T3-L1 cells (our unpublished data). Cotransfection of K8 with EYFP-K14R₁₂₅C resulted in the formation of keratin aggregates distributed throughout the whole cytoplasm, but not in filaments (Figure 2, A–C). Remarkably, if in addition wt K18 was cotransfected, mut EYFP-K14R₁₂₅C integrated into perinuclear filament bundles (Figure 2, D–F). Similar to the stable cell culture model (Figure 1), there was an apparent segregation of keratin aggregates in the cell periphery coexisting with keratin filaments in the cell center and a colocalization of wt keratins in the mutant-enriched aggregates. Thus, in absence of wt keratins of the same type, mut K14R₁₂₅C impairs formation of IF with a wt type II keratin. The extent to which mut keratin subunits are incorporated into filaments seems to depend on the ratio mut K14R₁₂₅C to wt keratin of the same type.

The K14R₁₂₅C Mutant Is Enriched in the Soluble Fraction without a type II Keratin Partner

The observation that the K14R₁₂₅C mutant segregated into distinct fractions and displayed limited assembly in cells, led us to examine its distribution within the insoluble and soluble cytoskeletal protein pools in cells by Western blotting. The amount of the K14R₁₂₅C mutant was similar to the expression of wt K14 in control cells and corresponded to 10–15% of total keratins in all cell lines examined (our unpublished data). Remarkably, in mut MCF-7 cells and HaCaT keratinocytes, there was a strong increase of mut K14R₁₂₅C protein in the soluble cytoskeletal fraction, detectable by GFP- and K14-specific antibodies (Figure 3, A and B, arrowheads), independently of the endogenous keratin pattern. In both cell lines, quantification of the bands revealed an amount of 52% of the mut K14 in the cytoskeletal and 48% in the soluble fractions. However, wt K14 in control-transfected cells was found exclusively in the insoluble cytoskeletal fractions. By using antibodies to endogenous keratins, no type II keratin partners, K8 or K5, were detected in the soluble fractions of MCF-7 and HaCaT cells, respectively. The occurrence of aggregates and filaments in the same cell prevented characterization of the polymerization status of keratin aggregates, which were resistant to high salt extraction in living cells (our unpublished data). Further

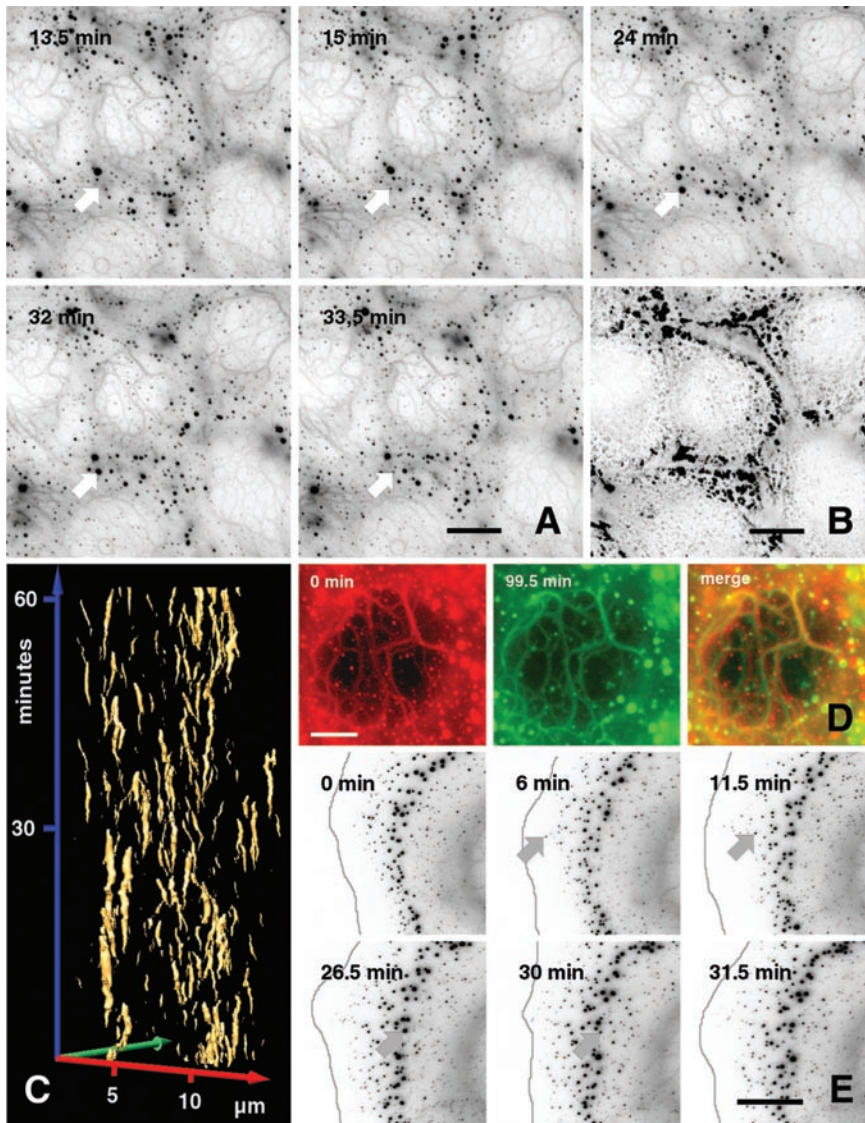


Figure 4. Time-lapse recordings of the mutant keratin cytoskeleton. (A) Images taken from a 99.5-min recording (Movie 1) of confluent growing EYFP-K14R₁₂₅C MCF-7 cells showing continuous turnover of aggregates. At each time point, a stack of six planes was recorded and projected into a single image. For better visualization, an inverse presentation was chosen. The white arrows point to the positions of a single representative aggregate that emerges and disappears during the recording time. Bar, 10 μ m. (B) Projection of the first 30 min from Movie 1 into a single picture depicting the area of aggregate turnover. (C) Time space diagram derived from a 60-min sequence of a time-lapse movie showing appearance and disappearance of aggregates in confluent growing EYFP-K14R₁₂₅C cells (Movie 1). The time is plotted along the blue axis in minutes, whereas the movement in the xy directions is plotted along the red and green axis in micrometers. The golden trajectories represent the surfaces of aggregates and show their emergence and disappearance. (D) Comparison of central filaments from a cell shown in Movie 1, depicting their stability over a time range of 99.5 min. The red and green image, representing the first and last frame of the movie, has been merged. Although aggregates show no overlap, the filaments remain in place during the recording time (yellow). (E) Images taken from a 31.5-min recording of EYFP-K14R₁₂₅C cells showing continuous turnover and inward movement of aggregates. For better visualization, an inverse presentation was chosen. The gray line represents the cell edge that was edited from bright-field images recorded in parallel. The arrow points to a single representative aggregate that occurs after 6 min, moves during the recording time toward the cell center, and finally disappears. Bars, 10 μ m (A and D) and 5 μ m (E).

fractionation of the soluble protein extracts into detergent-soluble and soluble cytoskeletal fractions revealed that a high amount of soluble K14R₁₂₅C protein was found in the detergent-soluble fraction. At any rate, K14R₁₂₅C, and most likely, other keratin mutations as well, raise the amount of soluble subunits in cells accompanied by impaired formation of IFs in cells.

Disease-Type Keratin Aggregates Are Transient Structures

Time-lapse recording of multiple Z-stacks revealed that newly formed small aggregates occurred near the cell periphery within 2 μ m of the tip of the lamellipodium, increased in diameter on their journey inwards and dissolved (Figure 4, A and E, arrow; Movies 1 and 2). Most significantly, and unexpected, they were not stable, but assembled and disassembled in a futile cycle with a half-life period of <15 min, as demonstrated by the time-space diagram (Figure 4C). Imaging of six Z-stacks further revealed that the aggregates fused with each other and dissolved again. The majority of aggregates was formed at the cell periphery and accumulated in the zone defined before by immunofluorescence analysis (Figure 1), also documented by the superposition of all single intakes of the film (Figure 4B).

In contrast to aggregates in the cell periphery, only a few small granules were detected in the central cytoplasm. These moved without clear trajectory and independent from perinuclear keratin filaments. Interestingly, the mobility of the K14R₁₂₅C-containing filaments was remarkably decreased in comparison with the cytoskeleton of control cells (Figure 4D; Movie 1). It is evident, that within ~100 min, mutant filaments did not display the slight undulatory movements typical of wt keratin filaments (Windoffer and Leube, 1999). With respect to *in vitro* studies (Ma *et al.*, 2001; Herrmann *et al.*, 2002), our findings support the concept that dominant keratin mutations alter the bundling properties, i.e., higher order structures of IFs but do not prevent their formation *per se*.

The average velocity of the uninterrupted uniform inward-flow of aggregates was 0.6 μ m/min; therefore, 6- to 10-fold increased in comparison with former studies on wt keratins in A431 and PtK2 epithelial cells (Windoffer and Leube, 1999; Yoon *et al.*, 2001), but lower than the speed of MT-dependent zigzag movement of wt EGFP-K5 particles (Liovic *et al.*, 2003). The dynamics of the mutant keratin aggregates coincided with the directionality and continuity of actin inward-flow in lamellipodial protrusions (Waterman-

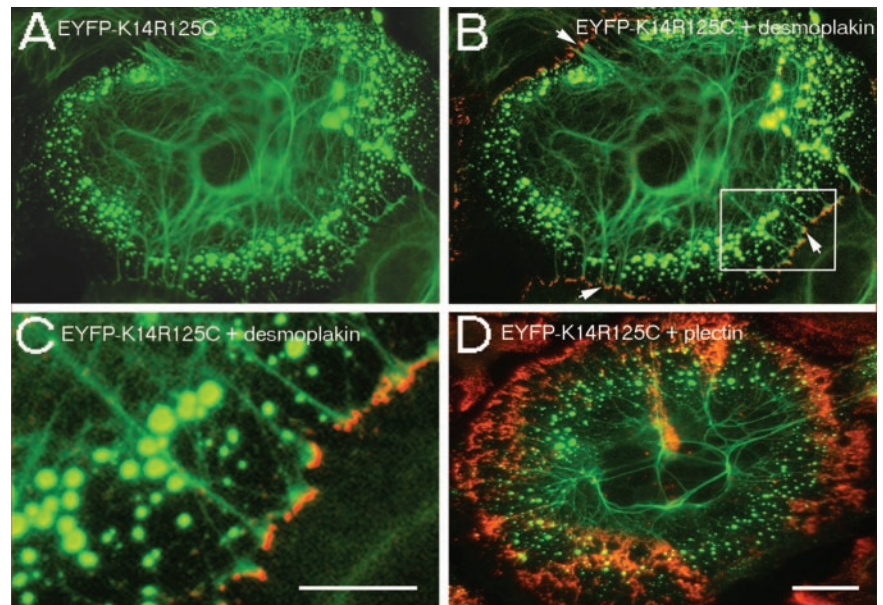


Figure 5. Localization of desmoplakin and plectin in mut HaCaT cells. (A) Expression of EYFP-K14R₁₂₅C. (B) Merged image of indirect immunofluorescence of desmoplakin (red) and EYFP-K14R₁₂₅C (green); the arrows mark the contacts of keratin filaments containing mut protein with desmosomes. (C) Higher magnification of the marked area in B. (D) Merged image of indirect immunofluorescence of plectin (red) and EYFP-K14R₁₂₅C (green). Bars, 5 μ m (C) or 10 μ m (A, B, and D).

Storer and Salmon, 1997), because the aggregates did not seem to follow fixed trajectories along rigid filaments, like MTs, and did not reveal the saltatory movements of an MT-dependent motor protein transport. Besides, immunofluorescence and electron microscopy data revealed that only few MTs extended to the outermost cell periphery but that they were displaced by a prominent subcortical actin meshwork (Figures 6, C–E, and 9A). The movement of keratin aggregates was energy dependent, because after ATP depletion, their motility stopped immediately (our unpublished data).

The presence of short IFs connecting some aggregates is in agreement with fluorescence and electron microscopy data (Figure 1H). Live cell imaging revealed the transient nature of some filamentous bridges between moving aggregates and provided additional evidence for the assembly deficiency of K14R₁₂₅C and its permanent exchange with the soluble pool of keratin subunits (our unpublished data).

Thus, the analysis of a mut, EYFP-tagged keratin in live cells has uncovered two novel and unexpected features of disease-type keratin aggregates: first, they are not static but highly dynamic and transient structures in contrast to the remarkably increased rigidity of mut filaments; and second, they form close to the plasma membrane and move toward the cell center.

Relationship of the K14R₁₂₅C Mutant to Desmosomes, Actin and Microtubule Cytoskeletons

The cytoskeleton and its major membrane anchorage sites, i.e., hemidesmosomes/desmosomes, adherens junctions, and focal contacts are regarded as an intricate protein meshwork. Therefore, we investigated whether the K14R₁₂₅C mutation affected the anchorage of IFs to desmosomes. Double fluorescence studies revealed no colocalization of keratin aggregates with desmoplakin. Furthermore, live cell imaging studies did not support a predominant incorporation of keratin precursors into IFs at desmosomes. Instead, bundles of keratin filaments, which contained mut EYFP-K14R₁₂₅C, reached the cell periphery and made contacts with desmoplakin-positive adhesion sites (Figure 5 B, arrows; and C).

To gain further insight into the molecular principles localizing keratin aggregates to a distinct region, the distribu-

tion of plectin, a candidate plakin mediating the interaction of IFs with MFs and MTs, was studied. The distribution of plectin in keratinocytes (Andra *et al.*, 2003), detected by an antibody, which recognizes an epitope in the rod domain common to many splice variants of plectin (Okumura *et al.*, 1999), was unaltered by the presence of keratin aggregates (Figure 5D).

Furthermore, double fluorescence studies were performed to study the distribution of EYFP-K14R₁₂₅C in correlation to MTs and MFs. There was no evidence for a colocalization of keratin aggregates with MTs, but the aggregates seemed to be located in the space between the MTs, although we cannot exclude a direct or indirect interaction with MTs by immunofluorescence analysis (Figure 6, C and D). The analysis of the actin cytoskeleton revealed that keratin aggregates were separated from the cell periphery by a prominent subcortical ring of F-actin (Figures 6E and 8A).

Thus, in contrast to vimentin particles, which have been detected in association with MTs in the peripheral region of spreading cells (Pralhad *et al.*, 1998), or a subspecies of small keratin granules which were shown to be associated with MT (Liovic *et al.*, 2003), we observed no colocalization of keratin aggregates with MTs or MFs.

Actin-dependent Inward-directed Transport of Keratin Particles

To date, studies on IF motility *in vivo* have focused on the interaction between IF subunits and MT-dependent motor proteins such as kinesin and dynein (Chou *et al.*, 2001; Helfand *et al.*, 2002). To elucidate the molecular basis for the inward transport of mut keratins, we performed live cell imaging in cells treated with MT- and MF-depolymerizing drugs.

Interestingly, the depolymerization of MT by nocodazole blocked neither the formation nor the rapid inward movement of keratin particles (Figure 7, A and B; Movie 3). The superposition of a peripheral section of all single intakes of the film revealed the unchanged continuous and directed inward movement of mut aggregates in the absence of MTs (Figure 7C). Even 6-h treatment did not induce a collapse of wt or mut keratin cytoskeletons (see supplemental figure).

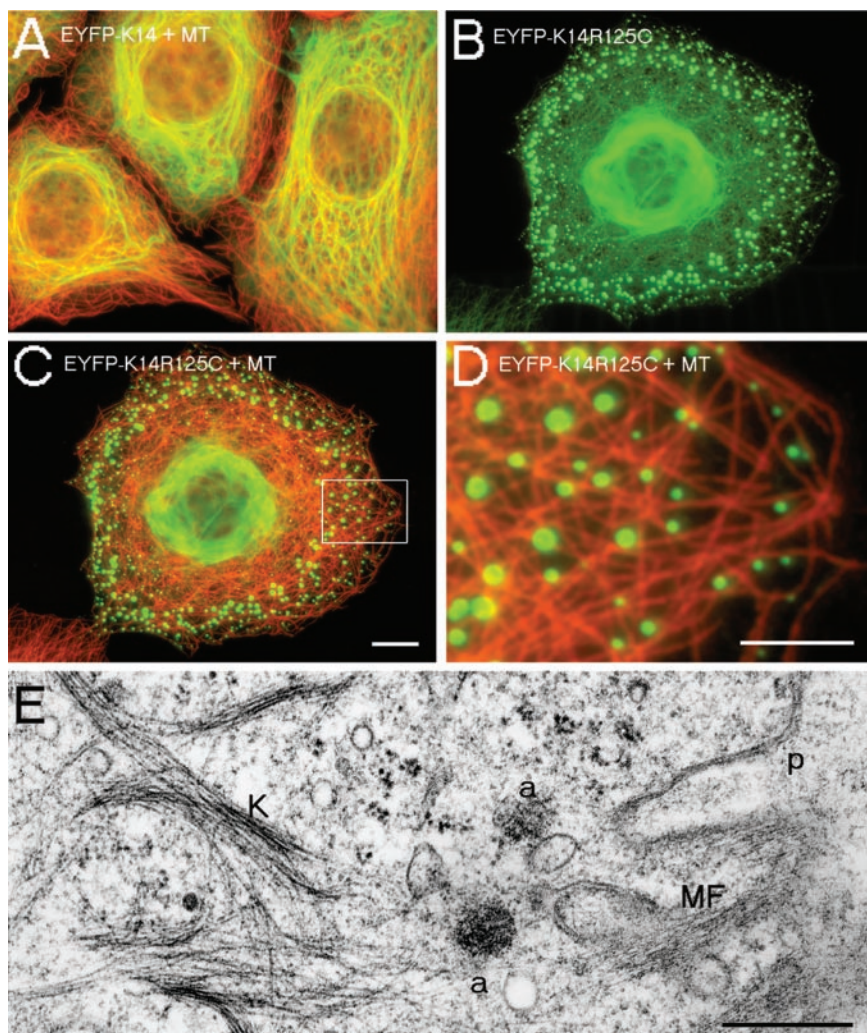


Figure 6. Localization of MTs and MFs in wt and mut MCF-7 cells. (A) Merged image of indirect immunofluorescence of MT (red) and EYFP-K14 (green). (B) Detection of EYFP-K14R₁₂₅C fluorescence in MCF-7 cells. (C) Merged image of indirect immunofluorescence of MT (red) and EYFP-K14R₁₂₅C (green). (D) Higher magnification of the marked area in C. (E) Electron microscopy of a EYFP-K14R₁₂₅C cell shows the distribution of keratin filaments (K), aggregates (a), and cortical MFs. p, plasma membrane. Bars, 5 μ m (D), 10 μ m (A–C), or 0.5 μ m (E).

We noted that upon depolymerization of MTs, keratin filaments showed a tendency to bundle, possibly reflecting a role of MTs or MT-associated proteins in the organization of keratins filaments.

Thus, at steady-state conditions, MT play no significant role in transport of mut keratin aggregates and the organization of the wt and mut keratin cytoskeletons in epithelial cells. However, they have an impact on the maintenance of the equilibrium between keratin filaments and soluble subunits, because Western blot data revealed an increase of soluble keratins (2%) in wt and mut cells after depolymerization of MT (see supplemental material).

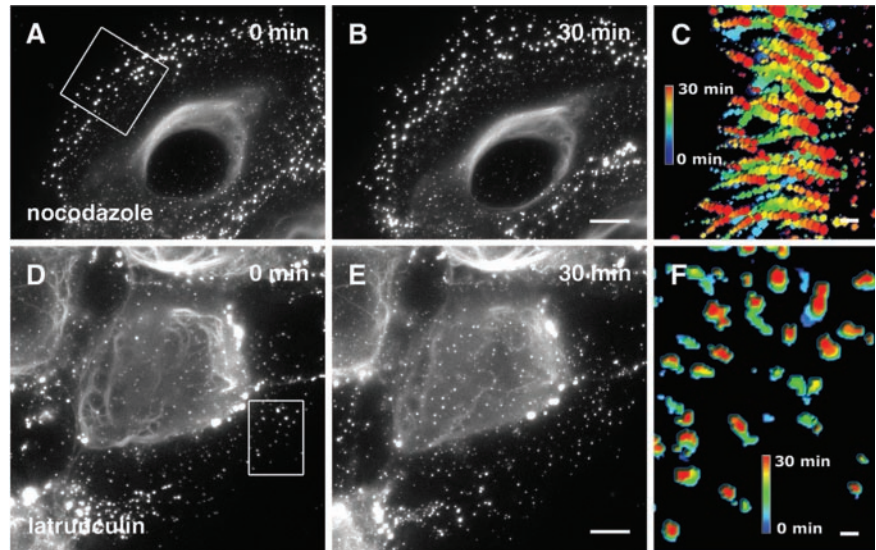
To gain an insight into the potential role of an actin-dependent transport of keratin particles, we studied the time course of latrunculin B and cytochalasin D action. In contrast to the treatment with nocodazole, both drugs elicited dramatic effects of the keratin cytoskeleton in live cells (Figure 7, D and E; Movies 4 and 5). Shortly after addition of 10 μ M latrunculin B, or 200 μ M cytochalasin D to cells, the flow of keratin aggregates toward the cell center stopped abruptly and only minimal residual motility of aggregates remained in the absence of intact MF as revealed by the superposition of a peripheral section of all single intakes of the film (Figure 7F). Furthermore, the formation of small keratin particles close to the plasma membrane ceased immediately. Given the toxicity of a combined treatment of the cells with MT-

and MF-depolymerizing drugs, the occurrence of unspecific side effects prevailed us from drawing the firm conclusion that MT are responsible for the residual motility. However, granules in the cell center, comparable with the MT-dependent particles reported by Liovic *et al.* (2003) remained motile and seemed transiently attached to the central keratin filaments, indicating the functionality of MT-dependent transport mechanisms in the absence of MFs.

In untreated cells, aggregates increased in size with growing distance from the cell periphery (Figure 8A). On prolonged presence of inhibitors, the zone containing keratin aggregates reversibly broadened from 5 to 40 μ m, whereas the cell body collapsed (Figure 8, A, B, and F). The fine, branched cell protrusions exclusively contained keratin aggregates, sometimes in proximity to MTs packed into thick bundles (Figure 8, F and G) or in close association with residual filamentous actin (Figure 8B, arrows). However, in the absence of intact MF, wt EYFP-K14 maintained its filamentous structure in spite of the altered cell morphology (Figure 8, C and D).

The recovery of cells from inhibitor treatment was accompanied by the reestablishment of the morphological and cytoskeletal reorganization in wt and mut cells within 1 h as keratin aggregates relocated near the cell periphery and the formerly described gradient of aggregate size from the cell

Figure 7. Time-lapse recordings of mut MCF-7 cells after treatment with nocodazole (Movie 3) and latrunculin B (Movie 4). Images of nocodazole-treated cells are taken from the first frame (A) and 30 min later (B) of Movie 3 starting 15 min after application of 40 μ M nocodazole. The first (D) and the last image (E) of Movie 4 starting 13.5 min after application of 10 μ M latrunculin B. (C and F) Visualization of aggregate tracks during the 30-min movie from selected areas (boxes in A and D). All movie frames of the selected areas were projected into single images and color coded in relation to time. Movement of aggregates after nocodazole treatment is shown as dotted lines in C, whereas standstill of aggregates after latrunculin B treatment is indicated by the absence of dotted lines in F. Bars, 10 μ m.



periphery toward the cell center was reestablished (Figure 8, E, H, and I).

In conclusion, the assembly and the inward-directed transport of mut keratin aggregates from the cell periphery inwards were largely dependent on an intact actin cytoskeleton. The residual minimal movement of keratin aggregates in F-actin-depleted cells may be due to a MT-dependent mechanism.

Osmotic Shock Reveals the Fragility of Rigid Filament Bundles in mut Epithelial Cells

To elucidate whether the altered cytoskeletal dynamics in mut cells had an impact on the resilience of mut cells to stress, we performed a hypoosmotic stress assay (D'Alessandro *et al.*, 2002). After incubation of cells in 150 mM urea, the keratin cytoskeleton of mut cells was susceptible to cell swelling, caused by the inward diffusion of the small permeant urea molecules followed by water. wt cells displayed an increased bundling of keratin filaments but showed hardly any cell deformation (Figure 9A). In contrast, the cytoskeleton in mut cells was partially disrupted and was distributed as aggregates in the cytoplasm (Figure 9B). This resulted in a stronger deformation of mut cells in comparison with wt cells. We assume that cells expressing an EBS hot-spot mutation and displaying altered dynamics of the keratin cytoskeleton are more susceptible to stress because of the rupture of mut filaments into aggregates, which are unable to maintain the normal cell morphology.

Mutation-specific Small Interfering RNAs Revert mut Keratin Network Morphology to the wt Phenotype

Given that live cell imaging studies revealed the transient nature of keratin aggregates, we reasoned that genetic interference with siRNAs might represent an appropriate tool for the treatment of EBS patients. Therefore, we engineered a K14R₁₂₅C-mut-specific siRNA containing one single nucleotide mutation-specific mismatch and carried out transient RNAi in wt and mut cells. Transfectants were analyzed 24, 48, 72, 96, and 120 h posttransfection. A maximum knock-down efficiency in up to 70% of cells, depending on the siRNA, was obtained within the time frame of 72–96 h. Wt EYFP-K14 fusion protein was suppressed by EYFP and K14 siRNAs, but not by the K14R₁₂₅C siRNA, which also had no

knock-down effect on endogenous wt keratins (our unpublished data). K14- and the mutant-specific siRNAs suppressed the expression of the K14R₁₂₅C protein completely, as judged by fluorescence microscopy (Figure 10).

The observation that cells treated with K14R₁₂₅C siRNA were devoid of aggregates demonstrated that their formation was dependent on the ratio of wt to mut protein. With respect to a potential therapy, it was important to know whether depletion of K14R₁₂₅C by the specific siRNA regenerated a normal, aggregate-free keratin cytoskeleton. Thus, after transfection of siRNAs, we performed immunofluorescence with antibodies to endogenous keratins. In cells transfected with K14R₁₂₅C siRNA, the wt keratin cytoskeleton was indistinguishable from that of untreated wt cells (Figures 1A and 10D). They were connected to untransfected mut cells by desmosomes, again confirming the functional integrity of desmosomes in the presence of aggregates (Figure 10D, arrows).

DISCUSSION

Research on keratins and IF in general has been guided by two dogmatic views, the first assuming that they represent stable, static structures and the second that their polymers, i.e., the IF cytoskeleton, results from a self-assembly process without need for accessory factors (Fuchs and Weber, 1994). At first glance, tissue fragility syndromes such as EBS and in vitro assembly data support the above-mentioned notion (Herrmann *et al.*, 2003). Recent live cell imaging studies based on GFP-tagged IF proteins are indicating that IFs, like other cytoskeletal polymers, are highly dynamic structures that require the association with motor proteins and kinases to fulfill their function (Chou and Goldman, 2000; Strnad *et al.*, 2001, 2002). Using EBS as a paradigm to investigate keratin function, we established stable epithelial cell lines expressing EYFP-tagged keratins as a model system to analyze the assembly and dynamics of mut keratins in living cells. The latter may have an impact on the instability of the cytoskeleton that cannot be detected in patient-derived cells. Because the stably transfected epithelial cell lines displayed a similar behavior to immortalized EBS keratinocytes in functional studies (D'Alessandro *et al.*, 2002), we consider HaCaT and MCF-7 cells as an appropriate model to analyze the EBS

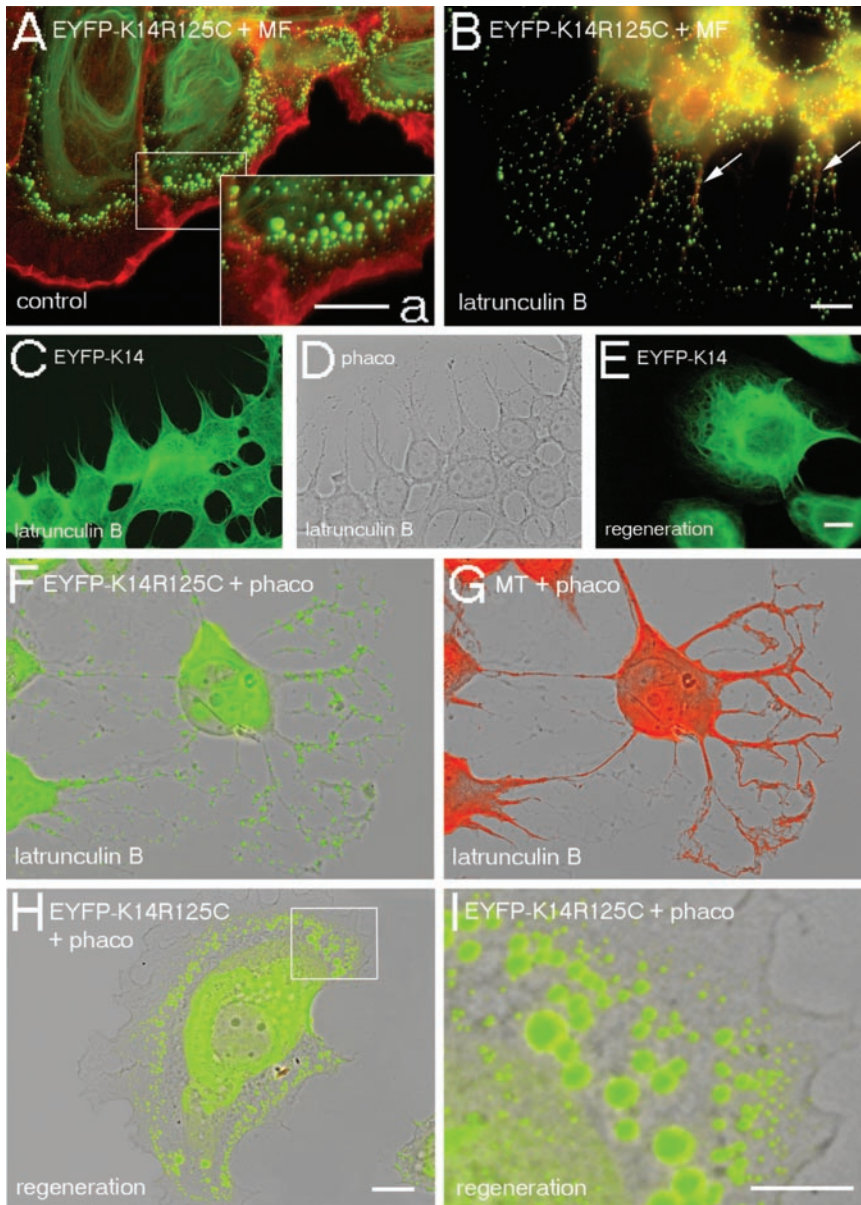


Figure 8. Dependence of keratin IFs from MFs. Double fluorescence analyses of wt and mut MCF-7 cells before (A), after the depolymerization of MFs by 10 μ M latrunculin B for 3 h (B–D, F, and G), or after subsequent regeneration of the cytoskeleton in latrunculin B-free culture medium for 1 h (E, H, and I). (A and B) Merged images of EYFP-K14R₁₂₅C (green) and Alexa 594-phalloidin fluorescence (red); the inset (a) shows a higher magnification of the area within the box in A. (C and E) EYFP-K14 fluorescence. (D) Corresponding phase contrast image. (F and H) Merged images of EYFP-K14R₁₂₅C fluorescence (green) and the corresponding phase contrast images. (G) Merged images of indirect immunofluorescence of tubulin (red) and the corresponding phase contrast image. (I) Higher magnification of the marked area in H. Bars, 5 μ m (a and I) or 10 μ m (A–H); same magnification in A, B, F–H, and C–E.

phenotype *ex vivo*. We arrived at three major conclusions: 1) Keratin “hot-spot” mutations such as K14R₁₂₅C lead to the formation of highly dynamic aggregates and decrease the intrinsic motility of filaments. 2) Keratin particles form close to the plasma membrane and are, in contrast to wt keratin precursors, transported toward the cell center in an actin-dependent mechanism. They accumulate in a distinct subcellular location. 3) The effect of a dominant-negative mutation is limited and fully reversible as demonstrated by RNAi studies. This may offer a rationale for the treatment of EBS.

The EBS Mutation K14R₁₂₅C Alters the Dynamic Properties of the Keratin Cytoskeleton

From a structural point of view, it is the formation of stable, cytotoxic keratin aggregates and a decrease in the number of normal IFs that cause keratinocyte and trophoblast fragility (Coulombe *et al.*, 1991a,b; Hesse *et al.*, 2000). Unlike previously assumed, *in vitro* assembly studies demonstrated that mutations such as K14R₁₂₅C do neither interfere with early

assembly stages nor obstruct the formation of IFs (Herrmann *et al.*, 2002). In support, Ma and coworkers pointed out that rheological properties exhibited by K5/K14R₁₂₅C-containing polymers were largely similar to those of the polymers from normal subunits (Ma *et al.*, 2001) but that mutations affect the higher order structure of filaments.

Our live cell studies offer a new and additional explanation for the mechanism by which keratin mutations lead to the EBS phenotype and revealed two different keratin fractions with distinct topology, mobility, and stability: a major mobile fraction in the cell periphery enriched in aggregates that turn over at a rapid rate and an extremely stable perinuclear array of keratin IFs that, in contrast to wt keratin filaments (Windoffer and Leube, 1999), displays a decreased intrinsic mobility (Figure 4). Until now, the formation of keratin aggregates in EBS has been regarded as a unidirectional process ending in insoluble structures. We show that at least in cultured epithelial cells, keratin aggregates are in

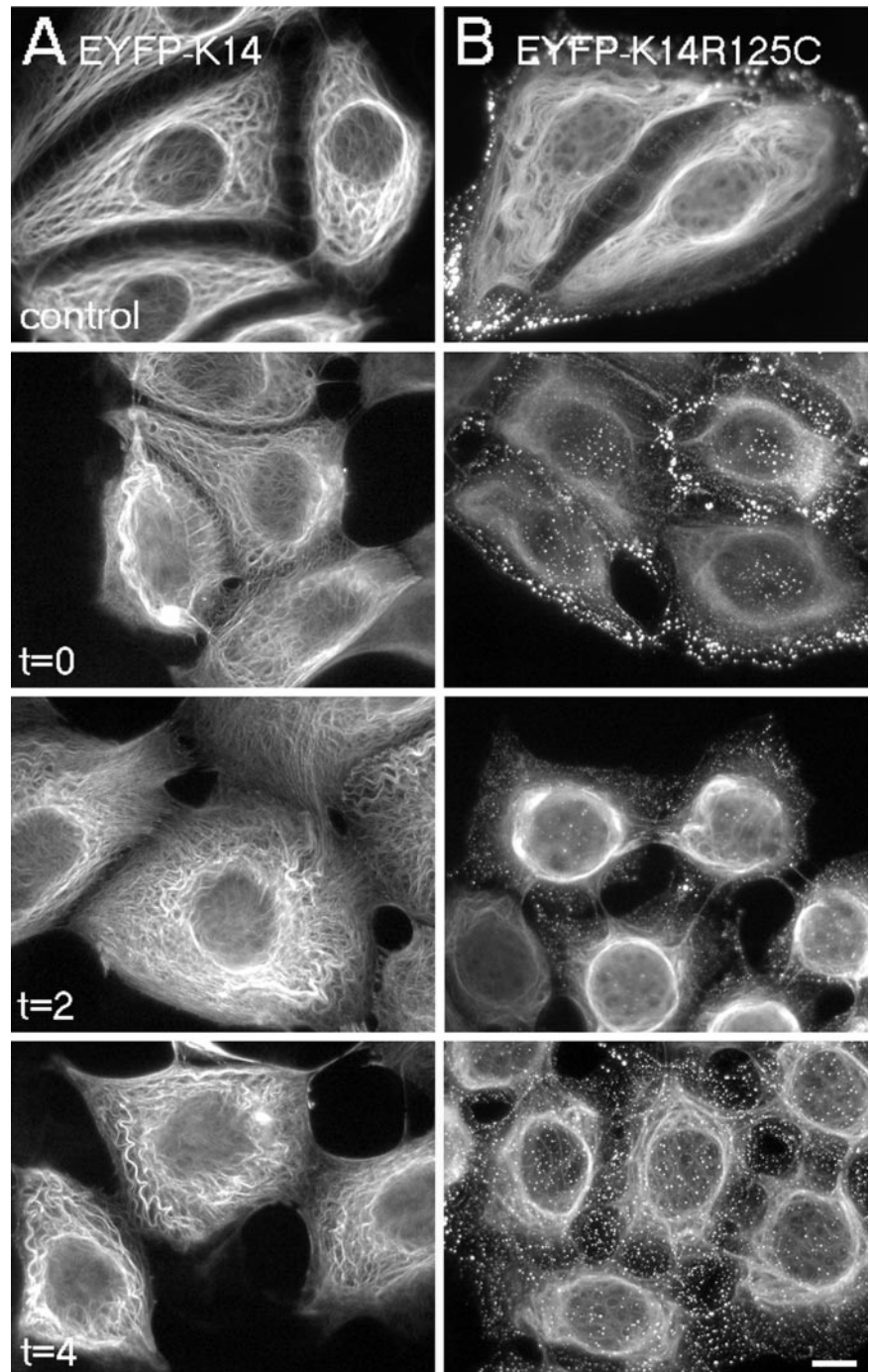


Figure 9. Osmotic shock. After incubation of cells in 150 mM urea in phosphate-buffered saline for 10 min, wt and mut cells were immediately fixed ($t = 0$) or regenerated in growth medium for the time indicated in the figure. (A) wt cells; the arrows mark desmosomes. (B) mut cells. Bar, 10 μm .

a continuous and rapid exchange with the soluble pool and do not represent insoluble debris.

In contrast, we show in the present study that although K14R₁₂₅C-containing keratin filaments seemed normal at the ultrastructural level, these filaments exhibited no longer the undulating movements typical of wt filaments (Windoffer and Leube, 1999; Yoon *et al.*, 2001) and displayed an unexpected stiffness. In functional studies applying osmotic stress on wt and mut cells, mut filaments displayed a higher fragility accompanied by increasing amounts of aggregates in the cytoplasm, resulting in larger cell deformation. We assume that the increased rigidity of mut filaments reflects *in vitro* findings that show altered bundling properties of

filaments built from mut subunits accompanied by a reduced capacity to withstand larger deformations (Ma *et al.*, 2001). Therefore, we suggest that not only mut aggregates, which are a common denominator of EBS, contribute to the phenotype but also the altered properties of mut filaments.

The Inward-directed Transport of Keratin Particles Is Mediated by an Actin-dependent Transport Mechanism

The assembly of keratin subunits into a three-dimensional cytoskeleton in cultured cells and *in vivo*, in contrast to MT and MF assembly, is only partly understood. Previous studies have already demonstrated the involvement of MT in the

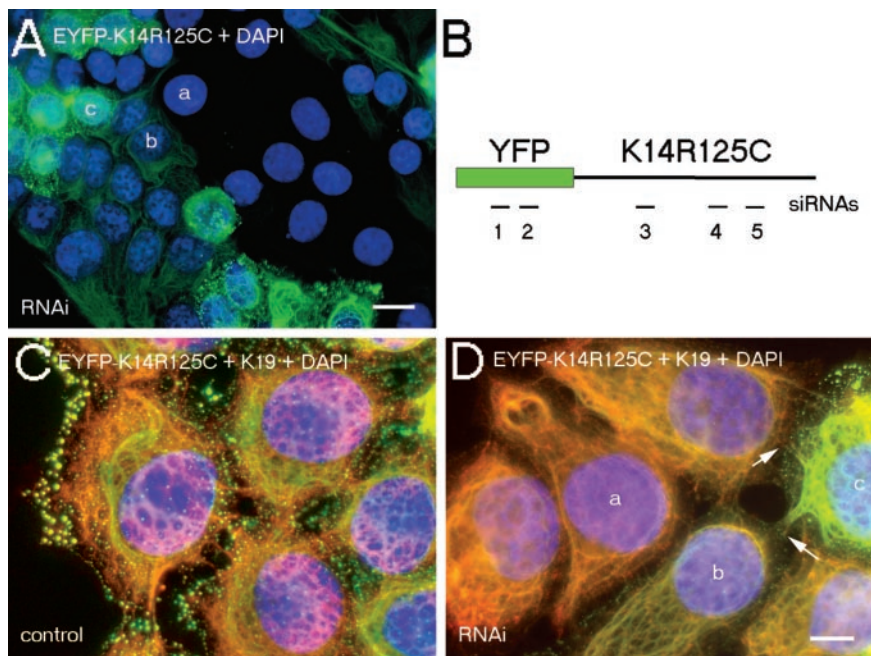


Figure 10. Suppression of mutant keratin by RNAi. Fluorescence analysis of mutant MCF-7 cells 96 h after transfection with K14-2 siRNA (A), or before (C) and after transfection with K14R₁₂₅C siRNA and subsequent indirect immunofluorescence with an antibody against K19 (D). (A) Merged images of EYFP-K14R₁₂₅C fluorescence (green) and 4,6-diamidino-2-phenylindole-stained DNA (blue). (C and D) Merged images of EYFP-K14R₁₂₅C (green), K19 fluorescence (red), and 4,6-diamidino-2-phenylindole-stained DNA (blue); the arrows mark desmosomes between mutant and suppressed cells. a, b, and c denote untransfected, partially suppressed, and completely suppressed cells, respectively. (B) Schematic view of the EYFP-K14R₁₂₅C mRNA with the positions of the siRNAs used in the RNAi experiments; the numbers correspond to the sequences given in MATERIALS AND METHODS. Bars, 20 μ m (A) and 10 μ m (C and D).

transport of keratin particles from the cell periphery inwards (Windoffer and Leube, 1999, 2001; Yoon *et al.*, 2001). We suggest that the aggregate zone in our mutant cells corresponds to the region in which the formation of keratin IFs from precursors (Herrmann *et al.*, 2003) takes place in epithelial cells. Although the early assembly steps are known to be rapid and unaffected by the K14R₁₂₅C mutation (Herrmann *et al.*, 2002), compaction of IFs is slower. Live cell imaging studies revealed that the transition from keratin particles to long IFs was impaired in a topologically restricted region in the cell periphery, despite of the presence of wt keratins. Moving toward the cell center, the aggregates increased in size and, sometimes, were transiently connected by short keratin filaments, consistent with the notion that the aggregates undergo the same process as wt IF precursors.

One of the most significant findings in our study is the steady flow of particles containing mutant and wt keratin from the plasma membrane toward the cell center, which is strictly dependent on the cortical actin cytoskeleton but not on MT-mediated dynamic transport processes. After the application of latrunculin B and cytochalasin D, both formation and inward-directed transport of keratin particles ceased instantly, suggesting that MF play a major role in these processes. As our movies revealed, there remained a residual movement of keratin aggregates for very small distances that might depend on a MT-based transport mechanism described by other studies. The importance of MFs for the keratin cytoskeleton is in agreement with studies demonstrating a dramatic reorganization of keratin filaments produced by cytochalasin D treatment and association of keratin with an as yet unspecified myosin and alpha-actinin (Wolf and Mullins, 1987), structural associations between keratin filaments and MFs (Knapp *et al.*, 1983), or keratin filaments and both MTs and MFs (Celis *et al.*, 1984). Our data on an actin-mediated assembly and transport are in agreement with studies in *Xenopus* egg extracts and activated eggs that also provided direct evidence for an association between MF and keratins *in vitro* and *in vivo*, indicating that this interaction contributes to proper keratin assembly (Weber and Bement, 2002). So, why does the mutant keratin not

display an MT-dependent inward transport? We suspect that the protein conformation in disease-type aggregates differs from wt precursors and, therefore, impairs the binding to MT adaptor or motor protein candidates. In this setting, actin-dependent transport mechanisms may gain a role in aggregate motility. At the margin of stationary cells, MF turn over very rapidly, recycling subunits for subsequent polymerization, which results into a retrograde flow away from the leading edge (Amann and Pollard, 2001). Therefore, we suppose a causal connection between the high actin polymerization activity in lamellipodial protrusions (Watanabe and Mitchison, 2002), keratin assembly in a distinct area near the plasma membrane, and the subsequent actin-mediated inward transport of keratin particles beginning within few microns away from the lamellipodial tip. Whether the inward-transport is mediated by actin-dependent motor proteins or whether it is a consequence of actin treadmilling as reported for actomyosin-based retrograde flow of MT in lamellipodia (Waterman-Storer and Salmon, 1997) remains to be elucidated in further studies.

Effect of a Dominant-Negative Mutation Is Limited and Fully Reversible as Demonstrated by RNAi Studies

Previous studies have reported that as little as 1–2% of mutant neurofilament subunits are sufficient to disrupt the cytoskeleton (Wong and Cleveland, 1990). We noted, however, that even 10–15% of the K14R₁₂₅C mutant did not completely disrupt a preexisting cytoskeleton but led to a segregation of peripheral aggregates and perinuclear filaments, both containing endogenous keratins. Presumably, the aggregates contained more mutant protein as the filaments, thereby forcing the endogenous proteins into aggregates. In the perinuclear region, where the concentration of polymerized endogenous wt protein was higher, substoichiometrical amounts of mutant K14R₁₂₅C integrated into the endogenous IFs. This interpretation is supported by transfection of wt and mutant keratin cDNAs into keratin-free preadipocytes. In this setting, the failure of mutant K14R₁₂₅C to form IFs with K8 can be rescued by cotransfection of wt K18. Thus, we conclude in agreement with similar observations in transgenic mice expressing mutant

K18 (Hesse and Magin, unpublished data) and heterozygous mut K14R₁₃₁C^{neo} mice bearing an EBS mutation equivalent to human K14R₁₂₅C (Cao *et al.*, 2001) that the ratio of mut to wt keratin dictates whether cytolysis prevails.

Here, we demonstrate for the first time that the specific down-regulation of mut keratin by siRNAs led to the reconstitution of a normal cytoskeleton. The fact that RNAi-treated cells were completely aggregate-free and reexpressed a normal endogenous keratin cytoskeleton confirmed our observations that the formation of aggregates in cells expressing mut K14R₁₂₅C was dependent on the ratio wt to mut protein. We note that partially suppressed cells still expressed mut K14R₁₂₅C, which remained integrated into the endogenous keratin filaments, but failed to disrupt it. Therefore, siRNA or small molecule approaches seem suitable to revert the effect of dominant keratin mutations in EBS. It is worth noting that in a *Drosophila* model of Huntington's disease, the formation of toxic protein inclusions and neurodegeneration could be reversed by the application of mimetic peptides (Kazantsev *et al.*, 2002).

In conclusion, the knockdown of mut protein by RNAi provided new insights into the characteristics of the EBS K14R₁₂₅C mutant and may offer a therapeutical approach for patients suffering from EBS.

ACKNOWLEDGMENTS

This work is dedicated to the late Peter Steinert. We thank Silke Loch for excellent technical assistance, and Jens Harborth and Klaus Weber (MPI of Biophysical Chemistry, Göttingen, Germany) for gifts of siRNAs and advice. This work was supported by the Deutsche Forschungsgemeinschaft grant FOR 367 (TP6) (to T.M.M.) and LE 566/7 (to R.E.L.), a grant from the Fonds der Chemischen Industrie (to T.M.M.), and the Bonner Forum Biomedizin.

REFERENCES

Amann, K.J., and Pollard, T.D. (2001). The Arp2/3 complex nucleates actin filament branches from the sides of pre-existing filaments. *Nat. Cell Biol.* 3, 306–310.

Andra, K., Kornacker, I., Jorgl, A., Zorer, M., Spazierer, D., Fuchs, P., Fischer, I., and Wiche, G. (2003). Plectin-isoform-specific rescue of hemidesmosomal defects in plectin (–/–) keratinocytes. *J. Invest. Dermatol.* 120, 189–197.

Anton-Lamprecht, I., and Schnyder, U.W. (1982). Epidermolysis bullosa herpetiformis Dowling-Meara. Report of a case and pathomorphogenesis. *Dermatologica* 164, 221–235.

Bachant, J.B., and Klymkowsky, M.W. (1996). A nontetrameric species is the major soluble form of keratin in *Xenopus* oocytes and rabbit reticulocyte lysates. *J. Cell Biol.* 132, 153–165.

Bader, B.L., Magin, T.M., Freudenmann, M., Stumpp, S., and Franke, W.W. (1991). Intermediate filaments formed de novo from tail-less cytokeratins in the cytoplasm and in the nucleus. *J. Cell Biol.* 115, 1293–1307.

Cao, T., Longley, M.A., Wang, X.J., and Roop, D.R. (2001). An inducible mouse model for epidermolysis bullosa simplex: implications for gene therapy. *J. Cell Biol.* 152, 651–656.

Celis, J.E., Small, J.V., Larsen, P.M., Fey, S.J., De Mey, J., and Celis, A. (1984). Intermediate filaments in monkey kidney TC7 cells: focal centers and interrelationship with other cytoskeletal systems. *Proc. Natl. Acad. Sci. USA* 81, 1117–1121.

Chou, C.F., Riopel, C.L., Rott, L.S., and Omary, M.B. (1993). A significant soluble keratin fraction in 'simple' epithelial cells. Lack of an apparent phosphorylation and glycosylation role in keratin solubility. *J. Cell Sci.* 105, 433–444.

Chou, Y.H., and Goldman, R.D. (2000). Intermediate filaments on the move. *J. Cell Biol.* 150, F101–F106.

Chou, Y.H., Helfand, B.T., and Goldman, R.D. (2001). New horizons in cytoskeletal dynamics: transport of intermediate filaments along microtubule tracks. *Curr. Opin. Cell Biol.* 13, 106–109.

Coulombe, P.A., Hutton, M.E., Letai, A., Hebert, A., Paller, A.S., and Fuchs, E. (1991a). Point mutations in human keratin 14 genes of epidermolysis bullosa simplex patients: genetic and functional analyses. *Cell* 66, 1301–1311.

Coulombe, P.A., Hutton, M.E., Vassar, R., and Fuchs, E. (1991b). A function for keratins and a common thread among different types of epidermolysis bullosa simplex diseases. *J. Cell Biol.* 115, 1661–1674.

Coulombe, P.A., and Omary, M.B. (2002). 'Hard' and 'soft' principles defining the structure, function and regulation of keratin intermediate filaments. *Curr. Opin. Cell Biol.* 14, 110–122.

D'Alessandro, M., Russell, D., Morley, S.M., Davies, A.M., and Lane, E.B. (2002). Keratin mutations of epidermolysis bullosa simplex alter the kinetics of stress response to osmotic shock. *J. Cell Sci.* 115, 4341–4351.

Elbashir, S.M., Harborth, J., Lendeckel, W., Yalcin, A., Weber, K., and Tuschl, T. (2001). Duplexes of 21-nucleotide RNAs mediate RNA interference in cultured mammalian cells. *Nature* 411, 494–498.

Fuchs, E., and Cleveland, D.W. (1998). A structural scaffolding of intermediate filaments in health and disease. *Science* 279, 514–519.

Fuchs, E., and Weber, K. (1994). Intermediate filaments: structure, dynamics, function, and disease. *Annu. Rev. Biochem.* 63, 345–382.

Gyoeva, F.K., and Gelfand, V.I. (1991). Coalignment of vimentin intermediate filaments with microtubules depends on kinesin. *Nature* 353, 445–448.

Harborth, J., Elbashir, S.M., Bechert, K., Tuschl, T., and Weber, K. (2001). Identification of essential genes in cultured mammalian cells using small interfering RNAs. *J. Cell Sci.* 114, 4557–4565.

Helfand, B.T., Mikami, A., Vallee, R.B., and Goldman, R.D. (2002). A requirement for cytoplasmic dynein and dynactin in intermediate filament network assembly and organization. *J. Cell Biol.* 157, 795–806.

Herrmann, H., Hesse, M., Reichenzeller, M., Aebi, U., and Magin, T.M. (2003). Functional complexity of intermediate filament cytoskeletons: from structure to assembly to gene ablation. *Int. Rev. Cytol.* 223, 83–175.

Herrmann, H., Wedig, T., Porter, R.M., Lane, E.B., and Aebi, U. (2002). Characterization of early assembly intermediates of recombinant human keratins. *J. Struct. Biol.* 137, 82–96.

Hesse, M., Franz, T., Tamai, Y., Taketo, M.M., and Magin, T.M. (2000). Targeted deletion of keratins 18 and 19 leads to trophoblast fragility and early embryonic lethality. *EMBO J.* 19, 5060–5070.

Ho, C.L., Martys, J.L., Mikhailov, A., Gundersen, G.G., and Liem, R.K. (1998). Novel features of intermediate filament dynamics revealed by green fluorescent protein chimeras. *J. Cell Sci.* 111, 1767–1778.

Irvine, A.D., and McLean, W.H. (1999). Human keratin diseases: the increasing spectrum of disease and subtlety of the phenotype-genotype correlation. *Br. J. Dermatol.* 140, 815–828.

Kazantsev, A., Walker, H.A., Slepko, N., Bear, J.E., Preisinger, E., Steffan, J.S., Zhu, Y.Z., Gertler, F.B., Housman, D.E., Marsh, J.L., and Thompson, L.M. (2002). A bivalent Huntingtin binding peptide suppresses polyglutamine aggregation and pathogenesis in *Drosophila*. *Nat. Genet.* 30, 367–376.

Kitajima, Y., Inoue, S., and Yaoita, H. (1989). Abnormal organization of keratin intermediate filaments in cultured keratinocytes of epidermolysis bullosa simplex. *Arch. Dermatol. Res.* 281, 5–10.

Knapp, L.W., O'Guin, W.M., and Sawyer, R.H. (1983). Rearrangement of the keratin cytoskeleton after combined treatment with microtubule and microfilament inhibitors. *J. Cell Biol.* 97, 1788–1794.

Kreitzer, G., Liao, G., and Gundersen, G.G. (1999). Detyrosination of tubulin regulates the interaction of intermediate filaments with microtubules in vivo via a kinesin-dependent mechanism. *Mol. Biol. Cell* 10, 1105–1118.

Letai, A., Coulombe, P.A., McCormick, M.B., Yu, Q.C., Hutton, E., and Fuchs, E. (1993). Disease severity correlates with position of keratin point mutations in patients with epidermolysis bullosa simplex. *Proc. Natl. Acad. Sci. USA* 90, 3197–3201.

Leube, R.E., Wiedenmann, B., and Franke, W.W. (1989). Topogenesis and sorting of synaptophysin: synthesis of a synaptic vesicle protein from a gene transfected into nonneuroendocrine cells. *Cell* 59, 433–446.

Leung, C.L., Green, K.J., and Liem, R.K. (2002). Plakins: a family of versatile cytolinker proteins. *Trends Cell Biol.* 12, 37–45.

Liovic, M., Mogensen, M.M., Prescott, A.R., and Lane, E.B. (2003). Observation of keratin particles showing fast bidirectional movement colocalized with microtubules. *J. Cell Sci.* 116, 1417–1427.

Ma, L., Yamada, S., Wirtz, D., and Coulombe, P.A. (2001). A 'hot-spot' mutation alters the mechanical properties of keratin filament networks. *Nat. Cell Biol.* 3, 503–506.

Martys, J.L., Ho, C.L., Liem, R.K., and Gundersen, G.G. (1999). Intermediate filaments in motion: observations of intermediate filaments in cells using green fluorescent protein-vimentin. *Mol. Biol. Cell* 10, 1289–1295.

- Okumura, M., Uematsu, J., Hirako, Y., Nishizawa, Y., Shimizu, H., Kido, N., and Owaribe, K. (1999). Identification of the hemidesmosomal 500 kDa protein (HD1) as plectin. *J. Biochem.* *126*, 1144–1150.
- Prahlad, V., Yoon, M., Moir, R.D., Vale, R.D., and Goldman, R.D. (1998). Rapid movements of vimentin on microtubule tracks: kinesin-dependent assembly of intermediate filament networks. *J. Cell Biol.* *143*, 159–170.
- Quinlan, R.A., Schiller, D.L., Hatzfeld, M., Achtstatter, T., Moll, R., Jorcano, J.L., Magin, T.M., and Franke, W.W. (1985). Patterns of expression and organization of cytokeratin intermediate filaments. *Ann. N.Y. Acad. Sci.* *455*, 282–306.
- Reichelt, J., Bussow, H., Grund, C., and Magin, T.M. (2001). Formation of a normal epidermis supported by increased stability of keratins 5 and 14 in keratin 10 null mice. *Mol. Biol. Cell* *12*, 1557–1568.
- Reichelt, J., Doering, T., Schnetz, E., Fartasch, M., Sandhoff, K., and Magin, T.M. (1999). Normal ultrastructure, but altered stratum corneum lipid and protein composition in a mouse model for epidermolytic hyperkeratosis. *J. Investig. Dermatol.* *113*, 329–334.
- Rosenbaum, J. (2000). Cytoskeleton: functions for tubulin modifications at last. *Curr. Biol.* *10*, R801–R803.
- Small, J.V., Stradal, T., Vignal, E., and Rottner, K. (2002). The lamellipodium: where motility begins. *Trends Cell Biol.* *12*, 112–120.
- Soellner, P., Quinlan, R.A., and Franke, W.W. (1985). Identification of a distinct soluble subunit of an intermediate filament protein: tetrameric vimentin from living cells. *Proc. Natl. Acad. Sci. USA* *82*, 7929–7933.
- Strnad, P., Windoffer, R., and Leube, R.E. (2001). In vivo detection of cytokeratin filament network breakdown in cells treated with the phosphatase inhibitor okadaic acid. *Cell Tissue Res.* *306*, 277–293.
- Strnad, P., Windoffer, R., and Leube, R.E. (2002). Induction of rapid and reversible cytokeratin filament network remodeling by inhibition of tyrosine phosphatases. *J. Cell Sci.* *115*, 4133–4148.
- Watanabe, N., and Mitchison, T.J. (2002). Single-molecule speckle analysis of actin filament turnover in lamellipodia. *Science* *295*, 1083–1086.
- Waterman-Storer, C.M., and Salmon, E.D. (1997). Actomyosin-based retrograde flow of microtubules in the lamella of migrating epithelial cells influences microtubule dynamic instability and turnover and is associated with microtubule breakage and treadmilling. *J. Cell Biol.* *139*, 417–34.
- Weber, K.L., and Bement, W.M. (2002). F-actin serves as a template for cytokeratin organization in cell free extracts. *J. Cell Sci.* *115*, 1373–1382.
- Windoffer, R., and Leube, R.E. (1999). Detection of cytokeratin dynamics by time-lapse fluorescence microscopy in living cells. *J. Cell Sci.* *112*, 4521–4534.
- Windoffer, R., and Leube, R.E. (2001). De novo formation of cytokeratin filament networks originates from the cell cortex in A-431 cells. *Cell Motil. Cytoskeleton* *50*, 33–44.
- Wolf, K.M., and Mullins, J.M. (1987). Cytochalasin B-induced redistribution of cytokeratin filaments in PtK1 cells. *Cell Motil. Cytoskeleton* *7*, 347–360.
- Wong, P.C., and Cleveland, D.W. (1990). Characterization of dominant and recessive assembly-defective mutations in mouse neurofilament NF-M. *J. Cell Biol.* *111*, 1987–2003.
- Yoon, K.H., Yoon, M., Moir, R.D., Khuon, S., Flitney, F.W., and Goldman, R.D. (2001). Insights into the dynamic properties of keratin intermediate filaments in living epithelial cells. *J. Cell Biol.* *153*, 503–516.
- Yoon, M., Moir, R.D., Prahlad, V., and Goldman, R.D. (1998). Motile properties of vimentin intermediate filament networks in living cells. *J. Cell Biol.* *143*, 147–157.